

Ground-state fidelity and quantum criticality in a two-leg ladder with cyclic four-spin exchange

Sheng-Hao Li,¹ Qian-Qian Shi,¹ Jin-Hua Liu,¹ and Huan-Qiang Zhou¹

¹Centre for Modern Physics and Department of Physics,
Chongqing University, Chongqing 400044, The People's Republic of China

We investigate a two-leg Heisenberg spin ladder with cyclic four-spin exchange by exploiting a newly-developed tensor network algorithm. The algorithm allows to efficiently compute the ground-state fidelity per lattice site, which enables us to establish the ground-state phase diagram for quantum lattice many-body systems. The latter is based on the observation that, for an infinite-size system, any singularity on a ground-state fidelity surface characterizes a critical point, at which the system undergoes a phase transition. For the two-leg Heisenberg spin-1/2 ladder with cyclic four-spin exchange, six different phases are identified: the ferromagnetic phase, the rung singlet phase, the staggered dimer phase, the scalar chirality phase, the dominant vector chirality region, and the dominant collinear spin region. Our findings are in a good agreement with the previous studies from the exact diagonalization and the density-matrix renormalization group.

PACS numbers: 74.20.-z, 02.70.-c, 71.10.Fd

Introduction. In the last decades, low-dimensional quantum spin systems, such as spin ladders, have been the subject of extensive experimental and theoretical interest. Many fascinating features of the ladder systems have long been understood theoretically from both analytical and numerical approaches [1, 2]. Among them is an intriguing property that the existence of an excitation gap depends on the number of legs: spin excitations are gapful for an even-leg ladder, and gapless for an odd-leg ladder. There are also a number of low-dimensional cuprate compounds of transition metals, whose properties are described adequately by multi-leg spin ladders. These ladder systems often exhibit some attractive properties such as quantum criticality. In addition, properties of several classes of materials such as $SrCu_2O_3$ [3], $La_6Ca_8Cu_{24}O_{41}$ [4], and $(C_5H_{12}N)_2CuBr_4$, are well described by a two-leg Heisenberg ladder with cyclic four-spin exchange.

On the other hand, a novel approach to critical phenomena in quantum many-body physics has emerged, based on the fact that fidelity, a basic notion in quantum information science, is a measure of quantum state distinguishability. The approach allows us to characterize critical phenomena in a variety of quantum many-body lattice systems in any spatial dimensions [5–14]. As argued in Refs. [6–11], the ground-state fidelity per lattice site is able to capture drastic changes of the ground-state wave functions around a critical point. This, in combination with the fact that many powerful numerical algorithms have been developed in the context of the tensor network (TN) representation, provides a powerful means to unveil quantum criticality underlying quantum many-body systems. In fact, a systematic scheme to study critical phenomena in quantum many-body lattice systems consists of three steps, as advocated in Ref. [15]: first, map out the ground-state phase diagram by computing the ground-state fidelity per lattice site; second, derive local order parameters (if any) from the reduced density matrices for a representative ground-state wave function in a given phase; third, characterize any phase without any long range order.

In this paper, we consider a two-leg Heisenberg spin-1/2 ladder with cyclic four-spin exchange. The ladder system ex-

hibits a very rich phase diagram, with six different phases identified: the ferromagnetic phase, the rung singlet phase, the staggered dimer phase, the scalar chirality phase, the dominant vector chirality region, and the dominant collinear spin region, when a properly chosen control parameter is varied. Therefore, the ladder system provides a test bed for our scheme to study quantum criticality in spin ladders. This is achieved by exploiting a newly-developed TN algorithm [16], which allows to efficiently compute the ground-state fidelity per lattice site, and the reduced density matrix from a representative ground-state wave function. Our findings are in a good agreement with the previous studies from the exact diagonalization [17, 18] and the density-matrix renormalization group (DMRG) [18].

Tensor network representation for spin ladders. The TN representation is a convenient way to represent ground-state wave functions in classical simulations of quantum many-body lattice systems, such as the matrix product state (MPS) [19–23] in one spatial dimension and the projected entangled-pair state (PEPS) [24–27] in two and higher spatial dimensions. Here, let us briefly recall the gradient TN algorithm to compute the ground-state wave functions for quantum many-body systems on an infinite-size two-leg spin ladder [16], adapted to be suitable to a system with cyclic four-spin exchange.

Assume that the Hamiltonian is translation-invariant: $H = \sum_i h^{[i]}$, with $h^{[i]}$ being the i -th plaquette Hamiltonian density along the leg direction. A TN representation for a quantum wave function consists of four-index tensors $A_{\ell rd}^s$, $B_{\ell rd}^s$, $C_{\ell ru}^s$, and $D_{\ell ru}^s$ attached to each site in the unit cell. Here, s is a physical index, $s = 1, \dots, \mathfrak{d}$, with \mathfrak{d} being the dimension of the local Hilbert space, and ℓ, r, u, d denote bond indices, $\ell, r, u, d = 1, \dots, \mathbb{D}$, with \mathbb{D} being the bond dimension. Then, for a random initial state $|\psi_0\rangle$, the energy is a functional of the TN tensors:

$$E = \frac{\langle \psi_0 | H | \psi_0 \rangle}{\langle \psi_0 | \psi_0 \rangle}, \quad (1)$$

which allows an efficient computation in the context of the TN representation. To update four-index tensors $A_{\ell rd}^s$, $B_{\ell rd}^s$, $C_{\ell ru}^s$,

and $D_{\ell ru}^s$, we need to compute the energy gradient,

$$\frac{\partial E}{\partial X_{\ell rd}^s} = \frac{1}{\langle \psi_0 | \psi_0 \rangle} \frac{\partial \langle \psi_0 | H | \psi_0 \rangle}{\partial X_{\ell rd}^s} - \frac{E}{\langle \psi_0 | \psi_0 \rangle} \frac{\partial \langle \psi_0 | \psi_0 \rangle}{\partial X_{\ell rd}^s}, \quad (2)$$

where $X_{\ell rd}^s \in \{A_{\ell rd}^s, B_{\ell rd}^s, C_{\ell ru}^s, D_{\ell ru}^s\}$. Once the energy gradient is known, the four-index tensors $A_{\ell rd}^s, B_{\ell rd}^s, C_{\ell ru}^s$, and $D_{\ell ru}^s$ may be updated as follows,

$$X_{\ell rd}^s = X_{\ell rd}^s - \delta \frac{\partial E}{\partial X_{\ell rd}^s}. \quad (3)$$

Here, δ denotes the step size during each iteration, which is tuned to be decreasing in the implementation, when the ground-state wave function is approached. Here, we stress that four different tensors $A_{\ell rd}^s, B_{\ell rd}^s, C_{\ell ru}^s$, and $D_{\ell ru}^s$ are updated simultaneously. Repeating this updating procedure until the ground-state energy converges, the system's ground-state wave function is generated in the TN representation. Actually, if the energy gradient $\frac{\partial E}{\partial X} \rightarrow 0$, a good approximation to the ground-state wave function is anticipated.

The model. The two-leg Heisenberg spin-1/2 ladder with cyclic four-spin exchange is described by the Hamiltonian:

$$H = J_{\perp} \sum_i S_{1,i} \cdot S_{2,i} + J_{\parallel} \sum_i (S_{1,i} \cdot S_{1,i+1} + S_{2,i} \cdot S_{2,i+1}) + K \sum_i (P_{i,i+1} + P_{i,i+1}^{-1}). \quad (4)$$

Here, $S_{\alpha,i}$ ($\alpha = 1, 2$) denotes the spin-1/2 Pauli operators at site i on the α -th leg, J_{\perp} is the interchain coupling between two spins on each rung, J_{\parallel} is the intrachain coupling between two neighboring spins in each chain, and K is the cyclic four-spin exchange interaction coupling. The cyclic four-spin permutation operator $P_{i,i+1}$ ($P_{i,i+1}^{-1}$) exchanges the four spins around the i -th plaquette as $S_{1,i} \rightarrow S_{1,i+1} \rightarrow S_{2,i+1} \rightarrow S_{2,i} \rightarrow S_{1,i}$, which can be decomposed in terms of the Pauli spin operators involving bilinear and biquadratic terms:

$$\begin{aligned} P_{i,i+1} + P_{i,i+1}^{-1} = & S_{1,i} \cdot S_{1,i+1} + S_{1,i+1} \cdot S_{2,i+1} + S_{2,i+1} \cdot S_{2,i} \\ & + S_{2,i} \cdot S_{1,i} + S_{1,i} \cdot S_{2,i+1} + S_{1,i+1} \cdot S_{2,i} \\ & + 4(S_{1,i} \cdot S_{1,i+1})(S_{2,i+1} \cdot S_{2,i}) \\ & + 4(S_{2,i} \cdot S_{1,i})(S_{1,i+1} \cdot S_{2,i+1}) \\ & - 4(S_{1,i} \cdot S_{2,i+1})(S_{1,i+1} \cdot S_{2,i}). \end{aligned} \quad (5)$$

The model has been investigated by the exact diagonalization [17, 28] and DMRG [17, 18, 29–31]. Here, we focus on the computation of the ground-state fidelity per lattice site in terms of the newly-developed TN algorithm. For simplicity, we choose $K = \sin \theta$, and $J_{\perp} = J_{\parallel} = \cos \theta$, with $\theta \in [-\pi, \pi]$.

The ground-state fidelity per lattice site. The ground-state wave function is generated from the newly-developed TN algorithm for a given choice of the coupling constants of the spin ladder, which allows to efficiently evaluate the ground-state fidelity per lattice site, a universal marker to detect quantum criticalities: a phase transition point is characterized by a pinch point on the fidelity surface.

For the two-leg Heisenberg spin ladder with cyclic four-spin exchange, we choose θ as a control parameter. For two different ground states, $|\psi(\theta_1)\rangle$ and $|\psi(\theta_2)\rangle$, corresponding to two different values θ_1 and θ_2 of the control parameter θ , the ground-state fidelity $F(\theta_1, \theta_2) = |\langle \psi(\theta_2) | \psi(\theta_1) \rangle|$ asymptotically scales as $F(\theta_1, \theta_2) \sim d(\theta_1, \theta_2)^N$, with N the total number of the lattice sites. Here, $d(\theta_1, \theta_2)$ is the scaling parameter, introduced in Refs.[6–8] for one-dimensional quantum lattice systems and in Refs.[9] for two and higher-dimensional quantum lattice systems. In fact, $d(\theta_1, \theta_2)$ characterizes how fast the fidelity goes to zero when the thermodynamic limit is approached. Physically, the scaling parameter $d(\theta_1, \theta_2)$ is the averaged fidelity per lattice site,

$$\ln d(\theta_1, \theta_2) \equiv \lim_{N \rightarrow \infty} \frac{\ln F(\theta_1, \theta_2)}{N}, \quad (6)$$

which is well defined in the thermodynamic limit even if $F(\theta_1, \theta_2)$ becomes trivially zero. It satisfies the properties inherited from the fidelity $F(\theta_1, \theta_2)$: (i) normalization $d(\theta, \theta) = 1$; (ii) symmetry $d(\theta_1, \theta_2) = d(\theta_2, \theta_1)$; and (iii) range $0 \leq d(\theta_1, \theta_2) \leq 1$.

In Fig.1, we plot a two-dimensional fidelity surface embedded in a three-dimensional Euclidean space for the two-leg Heisenberg spin-1/2 ladder with cyclic four-spin exchange. As shown in the upper panel, there are six pinch points on the fidelity surface, implying six phase transition points. In the lower panel, the contour plot of the ground-state fidelity per lattice site $d(\theta_1, \theta_2)$ on the (θ_1, θ_2) -plane is shown, with the truncation dimension up to 4. Therefore, we are able, by evaluating the ground-state fidelity per lattice site, to identify six different phases: the ferromagnetic phase, the rung singlet phase, the staggered dimer phase, the scalar chirality phase, the dominant vector chirality region, and the dominant collinear spin region. Notice that, among six transition points, there are two first-order phase transitions at $\theta \approx -0.40\pi$ and $\theta \approx 0.94\pi$ between ferromagnetic phase and its adjacent phases: the rung singlet phase and the dominant collinear spin region. The remaining four transition points are continuous. These results are in a good agreement with the earlier analyses [17, 18] based on the exact diagonalization and DMRG. Therefore, the TN algorithm yields reliable results for the two-leg Heisenberg spin ladder with cyclic four-spin exchange. In addition, the ground-state fidelity per lattice site, as a universal marker to detect phase transitions, is able to capture drastic changes of ground-state wave functions around critical points for quantum spin ladders.

Order parameters. Once the ground-state phase diagram is known, we are able to read out local order parameters (if any) from the reduced density matrices for a representative ground-state wave function in a given phase, as advocated in Ref. [15].

In the ferromagnetic phase, the non-zero-entry structure of the one-site reduced density matrix shows that the $\langle S_{\alpha,i} \rangle$ are the same at all the lattice sites for the two-leg spin ladder. Therefore, the local order parameter is

$$O_F = \langle \psi_0 | S_{\alpha,i} | \psi_0 \rangle. \quad (7)$$

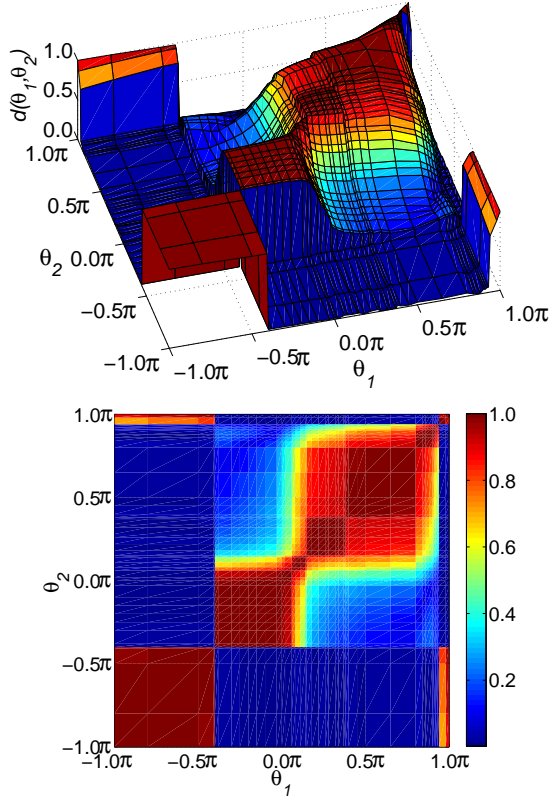


FIG. 1: (color online) Upper panel: A two-dimensional fidelity surface embedded in a three-dimensional Euclidean space. Lower panel: The contour plot of the ground-state fidelity per lattice site, $d(\theta_1, \theta_2)$, on the (θ_1, θ_2) -plane, for the two-leg Heisenberg spin-1/2 ladder with cyclic four-spin exchange. There are six pinch points on the fidelity surface. Therefore, six different phases are identified: the ferromagnetic phase, the rung singlet phase, the staggered dimer phase, the scalar chirality phase, the dominant vector chirality region, and the dominant collinear spin region. The ground-state phase diagram is as follows: the ferromagnetic phase for $-1.06\pi(0.94\pi) \lesssim \theta \lesssim -0.40\pi$, the rung singlet phase for $-0.40\pi \lesssim \theta \lesssim 0.06\pi$, the staggered dimer phase for $0.06\pi \lesssim \theta \lesssim 0.15\pi$, the scalar chirality phase for $0.15\pi \lesssim \theta \lesssim 0.38\pi$, the dominant vector chirality region for $0.38\pi \lesssim \theta \lesssim 0.80\pi$, and the dominant collinear spin region for $0.80\pi \lesssim \theta \lesssim 0.94\pi$.

As seen in Fig. 2), $|O_F| \equiv 0.50$. That is, spins are fully polarized in this phase. In fact, the spin correlations $\langle S_{\alpha,i} \cdot S_{\alpha,i+1} \rangle$ between the nearest-neighbor spins on the legs and the spin correlations $\langle S_{1,i} \cdot S_{2,i} \rangle$ between spins on the rungs are 0.25. The ferromagnetic state minimizes the energy on each plaquette separately for $-1.06\pi(0.94\pi) \lesssim \theta \lesssim -0.40\pi$.

In the rung singlet phase, the ground-state wave function may be approximated by the product of local rung singlets. The ground-state lacks long-range order in the conventional sense, thus there is no local order parameter; instead, an exotic order occurs. In fact, the rung singlet phase and the Haldane phase are essentially the same, namely, both are characterized by the so-called string order [32]. The rung singlet phase lies in $-0.40\pi \lesssim \theta \lesssim 0.06\pi$.

In the staggered dimer phase, the non-zero-entry structure

of the two-site reduced density matrix exhibits a pattern, with the local order parameter as follows,

$$O_{SD} = \frac{1}{2} \langle \psi_0 | S_{1,i-1} \cdot S_{1,i} - S_{1,i} \cdot S_{1,i+1} + S_{2,i} \cdot S_{2,i+1} - S_{2,i-1} \cdot S_{2,i} | \psi_0 \rangle. \quad (8)$$

Here, $\langle \psi_0 | S_{\alpha,i} \cdot S_{\alpha,i+1} | \psi_0 \rangle = \langle \psi_0 | S_{1,1} \cdot S_{1,2} | \psi_0 \rangle$ if $\alpha + i$ is even, $\langle \psi_0 | S_{\alpha,i} \cdot S_{\alpha,i+1} | \psi_0 \rangle = \langle \psi_0 | S_{2,1} \cdot S_{2,2} | \psi_0 \rangle$ if $\alpha + i$ is odd for two degenerate symmetry-breaking ground states in this phase. The ladder is in the staggered dimer phase for $0.06\pi \lesssim \theta \lesssim 0.15\pi$ (cf. Fig.2).

In the scalar chirality phase, we need to study the non-zero-entry structure of the three-site reduced density matrix. This yields the local order parameter

$$O_{SC} = \langle \psi_0 | S_{1,i} \cdot (S_{2,i} \times S_{1,i+1}) | \psi_0 \rangle. \quad (9)$$

It breaks the spatial symmetries and the time reversal symmetry, but not the internal SU(2) symmetry. The scalar chirality phase lies in $0.15\pi \lesssim \theta \lesssim 0.38\pi$, as seen from Fig.2.

In the dominant vector chirality region, the non-zero-entry structure of the two-site reduced density matrix yields the local order parameter

$$O_{VC-leg} = \langle \psi_0 | S_{\alpha,i} \times S_{\alpha,i+1} | \psi_0 \rangle, \quad (10)$$

$$O_{VC-rung} = \langle \psi_0 | S_{\alpha,i} \times S_{\alpha+1,i} | \psi_0 \rangle. \quad (11)$$

It breaks the spatial symmetries and the time reversal symmetry. In this phase, the spin correlations are strong between bonds on rungs and legs, but the spin correlations are very weak between diagonal bonds. The order parameter is plotted in Fig.2, which is non-zero between $0.38\pi \lesssim \theta \lesssim 0.80\pi$.

In the dominant collinear spin region, spins on the same leg exhibit ferromagnetic correlations, while spins on the same rung exhibit antiferromagnetic correlations. The non-zero-entry structure of the one-site reduced density matrix yields the local order parameter

$$O_{CS} = \frac{1}{2} \langle \psi_0 | S_{1,i} - S_{2,i} | \psi_0 \rangle. \quad (12)$$

The dominant collinear spin region lies in $0.80\pi \lesssim \theta \lesssim 0.94\pi$.

Therefore, we are able to “derive”, by investigating the non-zero-entry structure of the reduced density matrices for representative ground-state wave functions from different phases, the local order parameters for the ferromagnetic phase, the staggered dimer phase, the scalar chirality phase, the dominant vector chirality region and the dominant collinear spin region, with the order parameter O_F , O_{SD} , O_{SC} , O_{VC} and O_{CS} explicitly shown in Fig.2. In addition, no local order parameter is detected in the rung singlet phase, indicating that long range order is lacking in this phase. The ground-state phase diagram established from the local order parameters coincides with that from the ground-state fidelity per lattice site. That is, the ladder system undergoes four continuous phase transitions

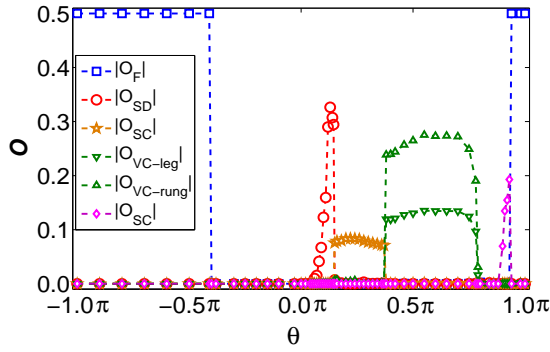


FIG. 2: (color online) The local order parameters O_F , O_{SD} , O_{SC} , O_{VC} , and O_{CS} in the ferromagnetic phase, the staggered dimer phase, the scalar chirality phase, the dominant vector chirality region, and the dominant collinear spin region versus θ , respectively.

at $\theta \approx 0.06\pi$, $\theta \approx 0.15\pi$, $\theta \approx 0.38\pi$ and $\theta \approx 0.80\pi$, and two first-order phase transitions at $\theta \approx -0.40\pi$ and $\theta \approx 0.94\pi$.

Conclusions. We have exploited a newly-developed efficient TN algorithm to compute ground-state wave functions for the two-leg Heisenberg ladder with cyclic four-spin exchange. We have mapped out, by computing the ground-state fidelity per lattice site, the phase diagram of the two-leg spin ladder with cyclic four-spin exchange. Six different phases are identified: the ferromagnetic phase, the rung singlet phase, the staggered dimer phase, the scalar chirality phase, the dominant vector chirality phase, and the dominant collinear spin phase. In addition, the corresponding local order parameters are “derived” from the reduced density matrices, which are computed efficiently in the context of the TN representation. Our findings are in a good agreement with the previous studies from the exact diagonalization [17, 18] and DMRG [18]. Therefore, the TN algorithm yields reliable results, and the ground-state fidelity per lattice site, as a universal marker to detect phase transitions, is able to capture drastic changes of ground-state wave functions around critical points, even for the two-leg Heisenberg spin ladder with cyclic four-spin exchange.

Acknowledgments. We thank Sam Young Cho, Bing-Quan Hu, Bo Li, Hong-Lei Wang, Ai-Min Chen, Yao-Heng Su, and Jian-Hui Zhao for enlightening discussions. This work is supported by the National Natural Science Foundation of China (Grant No: 10874252). SHL, QQS, and JHL are supported by Chongqing University Postgraduates’ Science and Innovation Fund (Project No.: 200911C1A0060322) and by the Fundamental Research Funds for the Central Universities (Project No. CDJXS11102214).

[1] T. Giamarchi, *Quantum Physics in One Dimension* (Oxford University Press, Oxford, 2004).
 [2] E. Dagotto and T. M. Rice, *Science* **271**, 618 (1996).
 [3] Y. Mizuno, T. Tohyama, and S. Maekawa, *J. Low. Temp. Phys.* **117**, 389 (1999).

[4] M. Matsuda, K. Katsumata, R. S. Eccleston, S. Brehmer, and H.-J. Mikeska, *Phys. Rev.* **62**, 8903 (2000).
 [5] P. Zanardi and N. Paunković, *Phys. Rev. E* **74**, 031123 (2006).
 [6] H.-Q. Zhou and J. P. Barjaktarević, *J. Phys. A: Math. Theor.* **41**, 412001 (2008).
 [7] H.-Q. Zhou, J.-H. Zhao, and B. Li, *J. Phys. A: Math. Theor.* **41**, 492002 (2008).
 [8] H.-Q. Zhou, arXiv:0704.2945.
 [9] H.-Q. Zhou, R. Orús, and G. Vidal, *Phys. Rev. Lett.* **100**, 080601 (2008).
 [10] J.-H. Zhao, H.-L. Wang, B. Li, and H.-Q. Zhou, *Phys. Rev. E* **82**, 061127 (2010).
 [11] H.-L. Wang, J.-H. Zhao, B. Li, and H.-Q. Zhou, arXiv:0902.1670.
 [12] P. Zanardi, M. Cozzini, and P. Giorda, *J. Stat. Mech.* L02002, (2007); N. Oelkers and J. Links, *Phys. Rev. B* **75**, 115119 (2007); M. Cozzini, R. Ionicioiu, and P. Zanardi, *Phys. Rev. B* **76**, 104420 (2007); L. Campos Venuti and P. Zanardi, *Phys. Rev. Lett.* **99**, 095701 (2007); T. Liu, Y.-Y. Zhang, Q.-H. Chen, and K.-L. Wang, *Phys. Rev. A* **80**, 023810 (2009).
 [13] W.-L. You, Y.-W. Li, and S.-J. Gu, *Phys. Rev. E* **76**, 022101 (2007); S. J. Gu, H. M. Kwok, W. Q. Ning, and H. Q. Lin, *Phys. Rev. B* **77**, 245109 (2008); M. F. Yang, *Phys. Rev. B* **76**, 180403(R) (2007); Y. C. Tzeng and M. F. Yang, *Phys. Rev. A* **77**, 012311 (2008); J. O. Fjårestad, *J. Stat. Mech.: Theory Exp.* (2008) P07011; J. Sirker, *Phys. Rev. Lett.* **105**, 117203 (2010).
 [14] M.M. Rams and B. Damski, *Phys. Rev. Lett.* **106**, 055701 (2011).
 [15] H.-Q. Zhou, arXiv:0803.0585.
 [16] S.-H. Li, Y.-H. Su, Y.-W. Dai, and H.-Q. Zhou, *Tensor network states for quantum spin ladders*, preprint.
 [17] A. Läuchli, G. Schmid, and M. Troyer, *Phys. Rev. B* **67**, 100409(R) (2003).
 [18] J.-L. Song, S.-J. Gu, and H.-Q. Lin, *Phys. Rev. B* **74**, 155119 (2006).
 [19] M. Fannes, B. Nachtergaele, and R. F. Werner, *Comm. Math. Phys.* **144**, 443 (1992); *J. Funct. Anal.* **120**, 511 (1994); S. Östlund and S. Rommer, *Phys. Rev. Lett.* **75**, 3537 (1995).
 [20] D. Perez-Garcia *et al.*, *Quantum Inf. Comput.* **7**, 401 (2007).
 [21] F. Verstraete, D. Porras, and J. I. Cirac, *Phys. Rev. Lett.* **93**, 227205 (2004).
 [22] G. Vidal, *Phys. Rev. Lett.* **91**, 147902 (2003); G. Vidal, *Phys. Rev. Lett.* **93**, 040502 (2004).
 [23] G. Vidal, *Phys. Rev. Lett.* **98**, 070201 (2007).
 [24] F. Verstraete and J. I. Cirac, arXiv:cond-mat/0407066.
 [25] V. Murg, F. Verstaete, and J. I. Cirac, *Phys. Rev. A* **75**, 033605 (2007).
 [26] J. Jordan *et al.*, *Phys. Rev. Lett.* **101**, 250602 (2008).
 [27] B. Li, S.-H. Li, and H.-Q. Zhou, *Phys. Rev. B* **79**, 060101(R) (2009).
 [28] K. Hijii and K. Nomura, *Phys. Rev. B* **65**, 104413 (2002).
 [29] Y. Honda and T. Horiguchi, arXiv:cond-mat/0106426.
 [30] T. Hikihara, T. Momoi, and X. Hu, *Phys. Rev. Lett.* **90**, 087204 (2003).
 [31] K. Hijii, S. Qin, and K. Nomura, *Phys. Rev. B* **68**, 134403 (2003).
 [32] M.P. M den Nijs and K. Rommelse, *Phys. Rev. B* **40**, 4709 (1989); S. R. White, *Phys. Rev. B* **53**, 52 (1996); E. H. Kim, Ö. Legeza, and J. Sólyom, *Phys. Rev. B* **77**, 205121(2008); M. Nakamura and S. Todo, *Phys. Rev. Lett.* **89**, 077204 (2002); G. Fáth, Ö. Legeza, and J. Sólyom, *Phys. Rev. B* **63**, 134403(2001).